PHYSICAL REVIEW B VOLUME 23, NUMBER 8 15 APRIL 1981

Uniaxial strain-dependent shallow donor polarizabilities. II. A new many-valley theoretical formulation

T. G. Castner and H. S. Tan*
University of Rochester, Rochester, New York 14627
(Received 27 October 1980)

A new many-valley theoretical formulation of the strain-dependent shallow donor polarizability is developed which should yield better agreement with experiment for the case when the $1s$-A_1–$1s$-E_a valley-orbit splitting $6\Delta(0)$ is much larger than the strain-induced splitting of the valleys. The ground-state wave function $\psi_{GS}(\vec{r},x)$, x the reduced valley strain, is taken as $\psi_{GS}(\vec{r},x) = \gamma(x)\psi_{A_1}(\vec{r},a_A(x)) + \beta(x)\psi_{E_a}(\vec{r},a_E(x))$ where $\gamma(x)$ and $\beta(x)$ are determined by the valley-repopulation model. $a_A(x)$ and $a_E(x)$ are strain-dependent Bohr radii, which differ by 16% for the P donor in Si for $x = 0$ and this difference grows with x. Unlike the previous approach each valley wave function component consists of two parts with different strain-dependent Bohr radii. $\psi_{GS}(\vec{r},x)$ is employed, using the Hassé method, to calculate the strain-dependent donor polarizability for P and Sb donors in Si. The results are compared to the experimental data for P and Sb donors in Si. For the isocoric P donor the new calculated results are in better agreement with the experimental results. However, one must still incorporate a strain-dependent valley-orbit splitting parameter $\Delta(x)$ to fit the experimental data. The results of the force-fit $\Delta(x)$ case show $a_A(x)$ increasing with x and the ground-state energy $E_{GS}(x)$ decreasing with x—both results are the opposite of those expected for the case $\Delta(x) = \Delta(0) = \text{constant}$. The donor piezohyperfine data of Wilson and Feher are reanalyzed utilizing independently measured values of $6\Delta(0)$ and the shear deformation potential Ξ_u. The results show that $a_A(x)$ must slowly increase with x, which is in qualitative agreement with the $a_A(x)$ increase inferred from the polarizability results.

I. INTRODUCTION

In the previous paper,[1] hereafter designated I, the uniaxial strain dependence of the shallow donor polarizability $\alpha_D(x)$, calculated employing the valley-repopulation model[2,3] (VRM) and different strain-dependent Bohr radii for the stress-raised and stress-lowered valleys,[4] is not in good agreement with the experimental data obtained from piezocapacitance measurements.[1] Although the calculated expression for $\alpha_D(x)$ can be force-fit to the data utilizing strain-dependent valley-valley coupling matrix elements, this approach is arbitrary and leads to large coefficients of the power series expansion of $\Delta(x)$ [$\Delta(x)$ is the adjacent valley coupling]. Furthermore, the slope of $\alpha_D(x)/\alpha_D(0)$ versus the reduced-valley strain x, as $x \to 0$, is only two-thirds of the experimental value for the P donor in Si despite the reasonable expectation that the VRM, with strain-dependent Bohr radii, would give good agreement with the data for very small strains. We shall formulate the theory differently, employing a bona fide many-valley approach with strain-dependent Bohr radii associated with the strain-coupled eigenstates rather than with the strain-shifted conduction-band valleys. This approach is preferable to the older approach given in I when the splitting of the strain-coupled eigenstates ($1s - A_1$ and $1s - E_a$) is large compared to the strain-induced splitting of the originally degenerate conduction-band minima. This is certainly the case for the substitutional donors P, As, Sb, and Bi in Si for the reduced-valley strain $|x| < 1$. On the other hand, the interstitial Li donor in Si has very small valley-valley coupling parameters[5] and might be expected to behave as expected by the conventional approach.

One of the difficulties confronted in comparing the experimental results for $\alpha_D(x)$ for the strain-dependent ground-state donor wave function with the calculated expressions results from the many effects, some of them interrelated, which occur when a crystal is subjected to uniaxial stress (or hydrostatic pressure). Even for the pure semiconductor there are small changes in the conduction-band-minima mass tensor[6] and in the host semiconductor dielectric constant[1,7] which slightly alter the conduction-band Bloch functions. These effects are proportional to the actual strain and the fractional changes ($\Delta m/m$ and $\Delta\epsilon_h/\epsilon_h$) are of order of the strain or smaller. However, the VRM effects and strain-induced changes in the donor envelope-function Bohr radii are much larger. In addition, as discussed qualitatively by Fritzsche,[4] changes in the individual valley envelope-function Bohr radii result in changes in the valley-valley coupling matrix elements. The complexity of the central-cell correction potential and the nonexponential decay of the donor envelope function[8] associated with the $1s$-A_1 state make it very difficult to reliably calculate the strain dependence of valley-valley coupling matrix elements. In this work we consider more carefully

how the Bohr radii and valley-valley coupling matrix elements change with strain in a self-consistent manner. The accumulation of a large body of data on a variety of uniaxial strain-dependent effects[9] in Si has led to a more reliable determination of the shear deformation potential Ξ_u. This in turn has permitted us to reanalyze the Wilson-Feher[3] donor piezohyperfine data and estimate how the Bohr radius of the $1s-A_1$ state changes under uniaxial compression. This change is shown to be qualitatively consistent with the changes in the $1s-A_1$ state Bohr radius inferred from the piezocapacitance data discussed in I and the new theory presented herein. This agreement of the new theoretical approach with different types of experimental data lends support to the new approach and suggests we can obtain quantitative information on the strain dependence of the valley-valley coupling matrix elements.

The approach developed below uses a many-valley ground-state wave function as the starting point for a variational calculation and thereby avoids the use of the single-valley parallel and perpendicular polarizability tensor components calculated by Dexter[10] and utilized in I as the basis for the theoretical expressions for $\alpha_D(x)$. Although some approximations will be made in the calculation of matrix elements, this new approach represents a partially self-consistent many-valley calculation of the strain-dependent donor polarizability.

The outline of the paper is as follows. In the next section the many-valley treatment of the strain-dependent donor polarizability is developed. An expression for the donor piezohyperfine Fermi contact interaction is also developed to compare with the Wilson-Feher[3] results. In Sec. III the experimental results will be compared with the new theoretical results. In Sec. IV we discuss the major conclusions and summarize the status of strain-dependent donor polarizabilities. Several appendices give the details of the matrix elements required for the calculation and a more general formulation of the valley-orbit matrix.

II. MANY-VALLEY TREATMENT OF STRAIN-DEPENDENT DONOR POLARIZABILITIES

A. Strain-dependent donor wave functions

Within the framework of the valley-repopulation model, the strain-dependent donor wave function for the αth eigenstate is generally written as

$$\psi_\alpha=\sum_i C_{\alpha i}(x)u_{\vec{k}_i}(\vec{r})e^{i\vec{k}_i\cdot\vec{r}}F_{\alpha i}(\vec{r},x)\,, \tag{1}$$

where $C_{\alpha i}(x)$ is a strain-dependent amplitude coefficient for the ith conduction-band valley, $u_{\vec{k}_i}e^{i\vec{k}_i\cdot\vec{r}}$ is the Bloch function at the ith valley minimum, and $F_{\alpha i}(\vec{r},x)$ is the strain-dependent envelope function associated with the ith valley. The reduced-valley strain x, using the well known deformation potential approach,[11] is given by

$$x_{100}=\frac{\Xi_u}{3\Delta(0)}(S_{11}-S_{12})\sigma_s\,, \tag{2a}$$

and

$$x_{110}=\frac{\Xi_u}{6\Delta(0)}(S_{11}-S_{12})\sigma_s \tag{2b}$$

for the stress σ_s (σ_s positive for a tensile stress) applied along the [100] and [110] axes, respectively. Ξ_u is the shear deformation, S_{11} and S_{12} are elastic compliance constants, and $6\Delta(0)$ is the zero-strain energy splitting of the $1s-A_1$ and $1s-E_a$ donor states. At zero strain the coefficients $C_{\alpha i}(0)$ are given by $C_{1s-A_1}=(1/6)^{1/2}(1,1,1,1,1,1)$ and $C_{1s-E_a}=(1/12)^{1/2}(-2,-2,1,1,1,1)$ for the $1s-A_1$ and the $1s-E_a$ states. These states are coupled by a [100] axis stress and lead to strain-dependent ground-state coefficients $C_{\mathrm{GS},i}(x)$ for the strain-dependent ground state of the form $C_{\mathrm{GS}-i}(x')=(C'_B,C'_B,C'_A,C'_A,C'_A,C'_A)$, where $C_A(x')$ and $C_B(x')$ are given by Eqs. (4a) and (4b) of I with $x=x_{110}$ replaced by $-x'=-x_{100}$. For a [110] axis stress, $C_{\mathrm{GS}-i}(x)$ takes the form $(C_A,C_A,C_A,C_A,C_B,C_B)$, with $C_A(x)$ and $C_B(x)$ given by Eqs. (4a) and (4b) of I.

We shall use the standard anisotropic envelope function[12] for a z-axis valley of the form

$$F_z(\vec{r})=\frac{1}{\sqrt{\pi a^2 b}}\exp\left[-\left(\frac{x^2+y^2}{a^2}+\frac{z^2}{b^2}\right)^{1/2}\right]$$
$$=\left(\frac{k^3 s^{1/2}}{\pi}\right)^{1/2}e^{-k(x^2+y^2+sz^2)^{1/2}}\,, \tag{3}$$

where k is proportional to a reciprocal Bohr radius and will have different strain-dependent values $k_A(x)$ and $k_B(x)$ for the $1s-A_1$ and $1s-E_a$ states of the strain-coupled pair of $1s$ states. The quantity $s=a^2/b^2=f(m_l/m_t)$ ($s=3.0278$ for Si for $m_l/m_t=4.8084$) will be considered a constant and independent of uniaxial strain along cubic or [110] axes. The use of a single Bohr radius for the $1s-A_1$ envelope function is not a particularly good approximation because of the strong central-cell correction, but may be an adequate approximation for the calculation of strain-dependent donor polarizabilities.

Rather than write the strain-dependent ground-state (GS) wave function in Eq. (1) as a sum over valleys, with each valley characterized by an $F_i(\vec{r},x)$ with a single strain-dependent Bohr radius, we shall write $\psi_{\mathrm{GS}}(\vec{r},x)$ as

$$\psi_{GS}(\vec{r},x)=\gamma(x)\psi_{A_1}(\vec{r},x)+\beta(x)\psi_{E_a}(\vec{r},x)\,, \tag{4}$$

where ψ_{A_1} and ψ_{E_a} contain the zero-strain coefficients C_{A_1} and C_{E_a} given above (we now drop the 1s since we consider only the 1s manifold of donor states). A comparison of Eqs. (1) and (4) for the same Bohr radii for each valley and for ψ_{A_1} and ψ_{E_a} yields the result

$$\gamma(x)=(\tfrac{2}{3})^{1/2}(2C_A+C_B),\ \text{and}\ \beta(x)=(\tfrac{4}{3})^{1/2}(C_A-C_B)\,. \tag{5}$$

One observes that $\gamma(x)$ decreases from 1 as x increases in magnitude while $\beta(x)$ increases linearly for a tension ($C_A'>C_B'$) and decreases linearly for a compression ($C_A'<C_B'$) for the [100] axis-stress case. For a [110] axis tension, $\beta(x)$ decreases ($C_A<C_B$).

The wave function $\psi_{GS}(\vec{r},x)$ in Eq. (4) is not the same wave function as Eq. (1) when the A_1 and E_a states have different Bohr radii. In particular if we view $\psi_{GS}(\vec{r},x)$ in Eq. (4) as a sum over the six conduction-band minima we find that each valley will have two components, rather than a single component in Eq. (1), one with a Bohr radius for the A_1 component and a different Bohr radius for the E_a component. The $+z$-valley component of ψ_{GS} in Eq. (4) will take the form

$$\psi_{GS,+z}=u_{k0}(\vec{r})e^{ik_0z}\left(\frac{\gamma(x)}{\sqrt{6}}F_z(\rho,z,s,k_A(x))+\frac{\beta(x)}{\sqrt{12}}F_z(\rho,z,s,k_E(x))\right), \tag{6}$$

where $\rho=(x^2+y^2)^{1/2}$, and the strain-dependent reciprocal Bohr radii $k_A(x)$ and $k_E(x)$ are given by

$$k_A(x)=\frac{3m_l\sqrt{s}}{m^*(s^2+2m_l/m_t)}\,\frac{1}{a_e}\left(\frac{E_{A_1}(x)-E_{cg}(x)}{E_{\text{ema}}}\right)^{1/2} \tag{7a}$$

and

$$k_E(x)=\frac{3m_l\sqrt{s}}{m^*(s^2+2m/m_t)}\,\frac{1}{a_e}\left(\frac{E_{E_a}(x)-E_{cg}(x)}{E_{\text{ema}}}\right)^{1/2}. \tag{7b}$$

In Eqs. (7a) and (7b), m^* is the isotropic mass which yields $E_{\text{ema}}=31.27$ meV (for Si) and a_e is the isotropic Bohr radius $a_e=a_B\epsilon_h(m/m^*)$. (For Si, $m^*=0.299$ and $a_e=20.18A$ for $\epsilon_h=11.40$.) The energies $E_{GS}(x)$, $E_{E_a}(x)$, and $E_{cg}(x)$ are the strain-dependent energies of the A_1 state, the E_a state, and the center of gravity of the six conduction-band valleys. For zero strain $k_A=1.03/a_e$ and $k_E=0.87/a_e$—a 16% difference which shows that the use of a single strain-dependent Bohr radius for this z valley is not a good approximation. The results for the [100] strain axis show $k_E(x)$ decreasing by $3\frac{1}{2}\%$ at $x_{100}=1$, compared to a much smaller 0.9% decrease in $k_{A_1}(x)$.

The two Bohr radii characterizing $\psi_{A_1}(x)$ and $\psi_{E_a}(x)$ become more different for a [100] axis tension as the tension increases. Thus, it is not a good approximation to replace the $F_z(\rho,z,k_A(x))$ and $F_z(\rho,z,k_E(x))$ in Eq. (6) by a single strain-dependent $F_z(\rho,z,k_z(x))$ and combine the two terms to obtain

$$[\gamma(x)/\sqrt{6}\,]^{1/2}+\beta(x)/(\sqrt{12})^{1/2}F_z(\rho,z,k_z(x))=C_A'(x)F_z\,,$$

where C_A' is obtained from Eqs. (5). On the other hand, if the valley-orbit splittings were negligible ($E_{E_a}\approx E_{A_1}$) then Eqs. (1) and (4) would yield virtually identical wave functions at small strain. The difference in the two approaches is that Eq. (4) places the emphasis on the eigenvalue rather than on the valley. When the two eigenvalues differ substantially in energy the eigenfunctions, characteristic of different sums over the valleys, should be characterized by different envelope functions with different Bohr radii. The Bohr radii are no longer associated with individual valleys. For donors with sizable valley-valley couplings and large chemical shifts Eq. (4) should be considerably more accurate than Eq. (1).

The strain dependence of $|\psi_{GS}(\vec{r}=0,x)|^2$ has been measured by Wilson and Feher[3] by measuring the uniaxial stress dependence of the donor hyperfine interaction. The Fermi contact hyperfine interaction $a_{hpf}(x)\propto|\psi_{GS}(\vec{r}=0,x')|^2$. Since $\psi_{E_a}(\vec{r}=0,x')=0$, Eqs. (3) and (4) yield

$$a_{hpf}(x)\propto\gamma(x')^2|u_{k0}(0)|^2k_A^3\sqrt{s}\,. \tag{8}$$

The $\gamma(x')^2$ factor will be that given Wilson and Feher[3] and is given by

$$\gamma(x')^2=1-\tfrac{1}{18}x'^2+\tfrac{1}{54}x'^3+\tfrac{1}{216}x'^4+\cdots. \tag{9}$$

Equation (9) gives the strain dependence of $a_{hpf}(x')/a_{hpf}(0)$ based on only the VRM, taking no account of changes in the Bohr radius $a_A(x)$ with strain. This was the procedure used by Wilson and Feher, who obtained values of $\Xi_u/6\Delta$ leading to Ξ_u values 14 to 25% larger than values obtained from piezoresistance[13,14] and piezo-optical[15] studies. However, Eq. (8), along with Eq. (7a) shows that $|\psi_{GS}(0,x')|^2$ also depends on the strain-dependent Bohr radius $a_{A_1}(x')$. We will show that one can explain the Wilson-Feher results for Si:P with $\Xi_u=8.6$ eV (Ref. 15) and $6\Delta=12.95$ (Ref. 16) by including a strain-dependent $a_{A_1}(x')$. Only a 0.5% increase in $a_{A_1}(x'=1)$ is required to explain the Wilson-Feher results for $a_{hpt}(x')/a_{hpf}(0)$.

B. Strain-dependent donor polarizabilities

The Hassé variational approach[17] is known to give an exact result for the polarizability of a hydrogen atom. This approach has been employed by Dexter[18] to calculate the magnetic-field dependence of the single-valley polarizability tensor components $\alpha_{\parallel}(H)$ and $\alpha_{\perp}(H)$ and also been used by Castner[19] in calculating the donor polarizability enhancement $\alpha_D(N)/\alpha_D(0)$ as $N \to N_c$, where N_c is the critical concentration for the onset of metallic behavior associated with the insulator-to-metal transition. For an electric field F applied along the z axis the trial wave function of Hassé is of the form

$$\psi_t = \psi_{GS}(\vec{r}, x)(1 + bz + crz) \tag{10}$$

and the Hamiltonian is of the form $H = H_D - eFz$. Minimization of the energy $E_t = \langle \psi_t | H | \psi_t \rangle / \langle \psi_t | \psi_t \rangle$ with respect to the variational parameters b and c leads to $E_{min} = E_{GS}(x) - \alpha_D(x)F^2/2$, where the donor polarizability $\alpha_D(x)$ is given by the expression

$$\alpha_D(x) = 2e^2 \frac{\lambda_1^2(B - \lambda_2 E_{GS}) + \lambda_3^2(A - \lambda_1 E_{GS}) - 2\lambda_1\lambda_3(C - \lambda_3 E_{GS})}{(A - \lambda_1 E_{GS})(B - \lambda_2 E_{GS}) - (C - \lambda_3 E_{GS})^2}, \tag{11}$$

where A, B, C, and E_{GS} are all strain-dependent matrix elements of H_D and λ_1, λ_2, and λ_3 are strain-dependent parameters given by $\lambda_1 = \langle z\psi_{GS} | z\psi_{GS} \rangle$, $\lambda_2 = \langle zr\psi_{GS} | zr\psi_{GS} \rangle$, and $\lambda_3 = \langle zr\psi_{GS} | z\psi_{GS} \rangle$. The matrix elements A, B, C, and E_{GS} are given, respectively, by $\langle z\psi_{GS} | H_D | z\psi_{GS} \rangle$, $\langle zr\psi_{GS} | H_D | zr\psi_{GS} \rangle$, $\langle zr\psi_{GS} | H_D | z\psi_{GS} \rangle$, and $\langle \psi_{GS} | H_D | \psi_{GS} \rangle$. $E_{GS}(x)$ is the strain-dependent donor ground-state energy and will play an important role in determining $\alpha_D(x)$ as can be seen from Eq. (11). The donor Hamiltonian H_D includes a central-cell correction (CCC) term $U_D(\vec{r})$ which is strongly donor-dependent and makes an important contribution to $E_{GS}(x)$. However, the contribution of $U_D(r)$ to A, B, and C will be neglected. This is an excellent approximation since the matrix elements A, B, and C contain extra factors (compared to E_{GS}) of r^2, r^4, and r^3 and therefore strongly emphasize the large-r outer portions of ψ_{GS} and de-emphasize the CCC from $U_D(\vec{r})$. The contribution to A from $U_D(r)$ is much less than 1% of the contribution from H_{EMA}.

In the present calculation the polarizability $\alpha_D(x)$ has been calculated in the limit as $\vec{F} \to 0$, i.e., for an infinitesimal electric field, but for a finite value of the strain. The trial wave function in Eq. (10) apparently does not include a specific contribution from an electric field-induced intervalley admixture, such as an admixture of the $1s - T_{2z}$ state. This omission is consistent with our neglect of all intervalley contributions to the matrix elements in Eq. (11) with the exception of those contributions to $E_{GS}(x)$. Thus, in the limit $|\vec{F}| = F_z = F \to 0$ the valley coefficients $C_{\alpha z}(x, F) = C_{\alpha' z}(x, F)$ and we believe the neglect of a specific intervalley admixture in ψ_t represents an excellent approximation.

Although it is possible to get an analytic expression for $\alpha_D(x)$ the expression would be very long and unwieldly. Since the calculations of $\alpha_D(x)/\alpha_D(0)$ were done numerically by computer, we shall discuss here a typical quantity $\lambda_1(x)$. The remaining quantities λ_2, λ_3, A, B, and C are given in Appendix A, but in fact all have the same type of functional dependence illustrated by $\lambda_1(x)$. Using Eq. (4), $\lambda_1(x)$ takes the form

$$\lambda_1(x) = \gamma^2(x) \langle z\psi_{A_1} | z\psi_{A_1} \rangle + \beta^2(x) \langle z\psi_{E_a} | z\psi_{E_a} \rangle + 2\gamma(x)\beta(x) \langle z\psi_{A_1} | z\psi_{E_a} \rangle . \tag{12}$$

For the [100] axis-stress case the three quantities $\langle z\psi_{A_1} | z\psi_{A_1} \rangle$, $\langle z\psi_{E_a} | z\psi_{E_a} \rangle$, and $\langle z\psi_{A_1} | z\psi_{E_a} \rangle$ are given by, if we neglect intervalley coupling terms,

$$\langle z\psi_{A_1} | z\psi_{A_1} \rangle = \tfrac{1}{3}(\langle zF_x | zF_x \rangle + \langle zF_y | zF_y \rangle + \langle zF_z | zF_z \rangle) = \tfrac{1}{3}\lambda_1^{\parallel}(k_{A_1}) + \tfrac{2}{3}\lambda_1^{\perp}(k_{A_1}), \tag{13a}$$

$$\langle z\psi_{E_a} | z\psi_{E_a} \rangle = \tfrac{1}{6}(4 \langle zF_x' | zF_x' \rangle + \langle zF_y' | zF_y' \rangle + \langle zF_z' | zF_z' \rangle) = \tfrac{1}{6}\lambda_1^{\parallel}(k_{E_a}) + \tfrac{5}{6}\lambda_1^{\perp}(k_{E_a}), \tag{13b}$$

$$\langle z\psi_{A_1} | z\psi_{E_a} \rangle = \frac{1}{3\sqrt{2}}(-2 \langle zF_x | zF_x' \rangle + \langle zF_y | 2F_y' \rangle + \langle zF_z | zF_z' \rangle) = \frac{1}{3\sqrt{2}}[\lambda_1^{\parallel}(k_A, k_E) - \lambda_1^{\perp}(k_A, k_E)], \tag{13c}$$

where F_i and F_i' differ because of the different values of $k_A(x)$ and $k_E(x)$ for the two eigenvalues. The quantities $\lambda_1^{\parallel} = \langle zF_z | zF_z \rangle$ and $\lambda_1^{\perp} = \langle zF_{x,y} | zF_{x,y} \rangle$ are the corresponding parallel and perpendicular single-valley parameters. The form of $\lambda_1(x)$ is finally given by

$$\lambda_1(x) = \gamma^2(x)[\tfrac{1}{3}\lambda_1^{\parallel}(k_A) + \tfrac{2}{3}\lambda_1^{\perp}(k_A)] + \beta^2(x)[\tfrac{1}{6}\lambda_1^{\parallel}(k_B) + \tfrac{5}{6}\lambda_1^{\perp}(k_B)] + \frac{\sqrt{2}}{3}\gamma(x)\beta(x)[\lambda_1^{\parallel}(k_A, k_B) - \lambda_1^{\perp}(k_A, k_B)] . \quad (14)$$

The cross term in Eq. (14) proportional to $\gamma(x)\beta(x)$ plays an important role in the strain-dependent behavior of $\alpha_D(x)$. It turns out that the parallel quantities (such as $\lambda_1^{\parallel}$) are $1/s$ times the perpendicular quantities (such as $\lambda_1^{\perp}$). As a result the cross terms containing $\gamma(x)\beta(x)$ will be a negative quantity times $\gamma(x)\beta(x)$. $\beta(x)$ is linear in x and changes sign from tension to compression. It is this term that accounts for the linear behavior of $\alpha_D(x)$ for small x. The quadratic behavior of the donor $a_{\text{hpf}}(x)/a_{\text{hpf}}(0)$ results since $\psi_{E_a}(r = 0, x) = 0$ and the $\beta(x)$ does not enter the expression for $a_{\text{hpf}}(x)$. However the linear behavior characteristic of $\alpha_D(x)$ is also characteristic of the piezohyperfine Fermi contact constants $a_{\text{hpf}}(\vec{r}_l, x)$ of Si^{29} nuclei at positions $\vec{r}_l$ with respect to the donor nucleus. In this case $\psi_{E_a}(\vec{r}_l, x) \neq 0$ (except for those Si^{29} nuclei lying along the various [111] axes) and the linear term proportional to $\gamma(x)\beta(x)$ plays an important role in determining the site-dependent magnitude of $\{[1/a_{\text{hpf}}(\vec{r}_l, x=0)] \times \partial a_{\text{hpf}}(\vec{r}_l, x)/\partial x\}_{x=0}$.

If one were to use isotropic envelope functions ($s = 1$) the quantity $[\lambda_1^{\parallel}(k_{A_1}, k_{E_a}) - \lambda_1^{\perp}(k_{A_1}, k_{E_a})]$ vanishes and the cross term effect would apparently vanish. However, when one takes account of the anisotropy and the fact that the x valleys move up and the (y, z) valleys move lower for a [100] axis tension, the coefficient of the $\gamma(x)\beta(x)$ term takes the form $[\lambda_1^{\parallel}(k_l) + \lambda_1^{\perp}(k_l) - 2\lambda_1^{\perp}(k_u)]$, where k_u and k_l are the inverse Bohr radii of the upper and lower valleys. Calculation of $\lambda_1(x)$ with Eq. (1) would yield

$$\lambda_1(x) = 2C_A^2[\lambda_1^{\parallel}(k_l) + \lambda_1^{\perp}(k_l)] + 2C_B^2\lambda_1^{\perp}(k_u) \quad (15)$$

which is to be compared with Eq. (14). If one converts this to $\lambda_1(x)$ in terms of the $\gamma(x)$ and $\beta(x)$ using Eqs. (5), it would look similar to Eq. (14). The real difference is in the different Bohr radii (k_A^{-1} and k_E^{-1}) which enter Eq. (14). Equation (15) starts out with the same Bohr radii for all the valleys at zero strain and contains only one Bohr radius per valley, not taking into account the anisotropy from $m_{\parallel}$ and $m_{\perp}$. Finally we re-emphasize that all the quantities A, B, C, and λ_2 and λ_3 have the same form as $\lambda_1(x)$, all having the same type of cross term. It only remains to discuss the behavior of $E_{GS}(x)$ and $E_{\text{“}E_a\text{”}}(x)$.

The energy in the effective-mass approximation is discussed in Appendix A for the zero-stress case. Clearly there will be no cross term $\gamma(x)\beta(x)$ since $\langle \psi_{E_a} | H_D | \psi_{A_1} \rangle = 0$. Solution of the coupled-valley equations (see Ref. 3) leads to results for $E_{GS}(x)$ and $E_{E_a}(x)$ of the form

$$E_{GS}(x) = -E_{\text{EMA}} - \Lambda - \Delta[2 + \delta - \tfrac{1}{2}x_{100} + \tfrac{3}{2}\phi(x_{100})] , \quad (16a)$$

and

$$E_{\text{“}E_a\text{”}}(x) = -E_{\text{EMA}} - \Lambda - \Delta[+2 + \delta - \tfrac{1}{2}x_{100} - \tfrac{3}{2}\phi(x_{100})] , \quad (16b)$$

where $\phi(x_{100}) = (4 + \frac{4}{3}x_{100} + x_{100}^2)^{1/2}$, Λ is the single-valley correction to EMA theory, Δ is the valley-valley coupling matrix element between adjacent valleys, while $\Delta(1 + \delta)$ is the valley-valley coupling matrix element between opposite valleys on the same cubic axis. These parameters are accurately known[20] for the shallow donors in Si and Ge. Equations (16a) and (16b) can be written in the form

$$E_{GS}(x) = -E_{\text{EMA}}\{1 + \eta + \xi[-\tfrac{1}{2}x_{100} + \tfrac{3}{2}\phi(x_{100}) - 3]\} \quad (17a)$$

and

$$E_{\text{“}E_a\text{”}}(x) = -E_{\text{EMA}}\{1 + \sigma + \xi[-\tfrac{1}{2}x_{100} - \tfrac{3}{2}\phi(x_{100}) + 3]\} , \quad (17b)$$

where $\eta = [\Lambda + \Delta(5 + \delta)]/E_{\text{EMA}}$, $\sigma = [\Lambda + \Delta(-1 + \delta)]/E_{\text{EMA}}$, and $\xi = \Delta/E_{\text{EMA}}$. In this form one observes that the strain dependence of both $E_{GS}(x)$ and $E_{E_a}(x)$ both depend only on the parameter ξ (or Δ). Both square brackets [ ] are zero at $x_{100} = 0$ but the square bracket in $E_{GS}(x)$ is small and positive while that in $E_{\text{“}E_a\text{”}}(x)$ is larger in magnitude and negative. It should also be noted that both $E_{GS}(x)$ and $E_{\text{“}E_a\text{”}}(x)$ are measured with respect to the center of gravity $E_{cg}(x) = (S_{11} + 2S_{12})(\Xi_d + \frac{1}{3}\Xi_u)\sigma_s$ of the six conduction-band minima. Thus the reciprocal Bohr radii $k_{A_1}(x)$ and $k_{E_a}(x)$ are proportional to the respective curly brackets in Eqs. (17a) and (17b). With η and ξ constant, $E_{GS}(x)$ becomes more negative with positive x_{100} (tension) and $k_A(x) \propto [-E_{GS}(x)/E_{\text{EMA}}]^{1/2}$ increases corresponding to a decrease in $a_{A_1}(x)$ which is contrary to both the polarizability data for $\alpha_D(x_{100})$ and to the donor hyperfine constant $a_{\text{hpf}}(x)$. However, as discussed by Fritzsche,[4] the valley-valley coupling matrix elements Δ and $\Delta(1 + \delta)$ both depend on the stress-dependent Bohr radii. These matrix elements depend critically on the central-cell potential $U_D(r)$, the envelope functions at small r, and how they change with strain. It is doubtful one can do a reliable calculation of $\Delta(x)$. Instead we shall assume a power series of from $\Delta(x) = \Delta(0)(1 + \sum_{t=1}^{n} C_t x^t)$. The C_t will be chosen to fit the polarizability data $\alpha_D(x_{100})$ and $\alpha_D(x_{110})$ and will then be

compared with each other for consistency and compared with the donor hyperfine data. The above analysis, only for the [100] axis stress, can readily be extended to the [110] axis case. The expressions for the quantities $\lambda_1(x_{110})$, etc., are discussed briefly in Appendix B.

III. STRAIN-DEPENDENT DONOR POLARIZABILITY RESULTS

Using Eq. (11) the strain-dependent donor polarizabilities $\alpha_D(x)$ have been calculated numerically versus the reduced valley strain x for [100] and [110] axis cases. Figure 1 shows the calculated results for $\alpha_D(x_{100})/\alpha_D(0)$ for the isolated P donor in Si for the [100] axis tensile-stress case. The solid curve VRM-EMA is that for the valley-repopulation model with a constant $E_{GS}(x) = E_{EMA} = 31.27$ meV. The slope is only about two-thirds of the experimental slope (• indicates the experimental points) and the curve shows a flattening at larger x, but exhibits no minimum out to $x \sim 0.9$. On the other hand the $[\mathrm{VMR}]_{\Delta(0)}$ curve [with $E_{GS}(x_{100})$ given by Eq. (16a) for $\Delta(x) = \Delta(0) =$ constant $= 2.16$ meV] shows almost the correct slope, but falls well below the experimental curve at $x_{100} \sim 0.5$ and also shows no sign of the minimum shown by the experimental data. By assuming all the valley-valley coupling matrix elements have the same reduced-valley strain dependence as the adjacent valley-valley matrix element

$$\Delta(x_{100}) = \Delta(0)(1 + C_1 x_{100} + C_2 x_{100}^2 + C_3 x_{100}^3 + \cdots),$$

the data can be fit very well for $C_1 = 0.01$, $C_2 = -0.145$, and $C_3 = 0.042$ (the calculated points are given by the x points). Using the theoretical approach given in I and a strain-dependent $\Delta(x_{100})$ the experimental data in Fig. 1 can be fit with $C_1 = 0.101$, $C_2 = -0.236$, $C_3 = 0.068$. These coefficients are considerably larger than those above obtained using Eqs. (10) and (11). The much larger C_1 actually yields a different qualitative behavior of $E_{GS}(x_{100})$. In the treatment given in I, $E_{GS}(x_{100})$ initially becomes greater in magnitude (negative), passes through a minimum in the vicinity of $x_{100}^{\min}$, and then increases (becoming smaller in magnitude). Using the approach in this paper, $E_{GS}(x_{100})$ is flat for small x_{100} and then slowly rises [decreasing in magnitude (see Fig. 7)]. Thus, the qualitative behavior of the two approaches differs for $x_{100} < x_{100}^{\min}$ but is similar for $x_{100} > x_{100}^{\min}$.

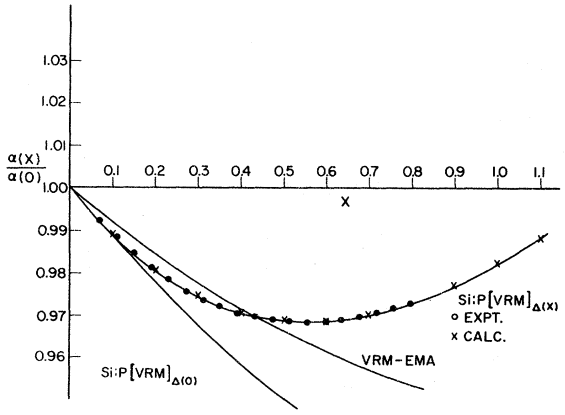

FIG. 1. $\alpha_D(x_{100})/\alpha_D(0)$ vs x_{100} for the isolated P donor in Si. The VRM-EMA curve is for $E_{GS}(x) = E_{EMA} =$ constant. The $[\mathrm{VRM}]_{\Delta(0)}$ curve is for $E_{GS}(x)$ given by Eq. (16a). The $[\mathrm{VRM}]_{\Delta(x)}$ curve is for $\Delta(x) = \Delta(0)\,(1 + 0.01x - 0.145\,x^2 + 0.042\,x^3)$.

One might argue that force-fitting these two different theoretical approaches to the data does not give one a basis for reliably choosing between the two theories. The fact that the C_i's are smaller (C_1 is much smaller) in the new approach is hardly a convincing argument for choosing between the two approaches. However, the smallness of C_1 in the new approach is suggestive. While a first-principles self-consistent calculation of $\Delta(x_{100})$ is beyond the scope of the present work it is clear that $\Delta(x_{100})$ depends on $a_A(x_{100})$ and $a_E(x_{100})$ [$a_u(x_{100})$ and $a_l(x_{100})$ in the approach in I] and that these quantities in turn depend on $\Delta(x_{100})$ through Eqs. (7) and (16). It is reasonable to assume that $\Delta(x_{100})$ depends predominantly on the core part of the envelope function and that this part of the envelope function is somewhat less sensitive to strain than the outer part for $|\vec{r}| \sim a_A(x_{100})$. In fact our reanalysis of the Wilson-Feher $a_{hpf}(x)/a_{hpf}(0)$ data definitely supports this view. This being the case, then a small C_1 in $\Delta(x_{100})$ would be more plausible.

For the [110] axis tensile-stress case one might expect similar behavior with x_{100} replaced by x_{110} [but note in C_A and C_B given in Eqs. (4a) and (4b) of I that x_{100} must be replaced by $-x_{110}$]. However, this change in sign in the $C_A(x)$ and $C_B(x)$ does give a different power-series expansion for $\gamma(x_{110})$ than for $\gamma(x_{100})$ and the two cases are not expected to be identical. However, it is worth checking what sort of fit one obtains if one uses the c_j above for $\Delta(x_{100})$ which gave an excellent fit for $\alpha_D(x_{100})/\alpha_D(0)$ for the [100] case. Figure 2 shows the [110] axis data for $\alpha_D(x_{110})/\alpha_D(0)$ vs x_{110} [note the electric field was along the z axis and the experiment determined $\alpha_{D,zz}(x_{110})/\alpha_D(0)$]. Also shown in Fig. 2 are the calculated curves for $\alpha_D(x_{110})/\alpha_D(0)$ for the two cases $C_1 = C_2 = C_3 = \cdots = 0$ [$\Delta(x_{110}) = \Delta(0) =$ constant], and secondly for $C_1 = 0.01$, $C_2 = -0.145$, and $C_3 = 0.042$. The data is almost linear out to $x \sim 0.4$ but shows a slight upward deviation from linearity for larger values of x_{110}. The calculated curve

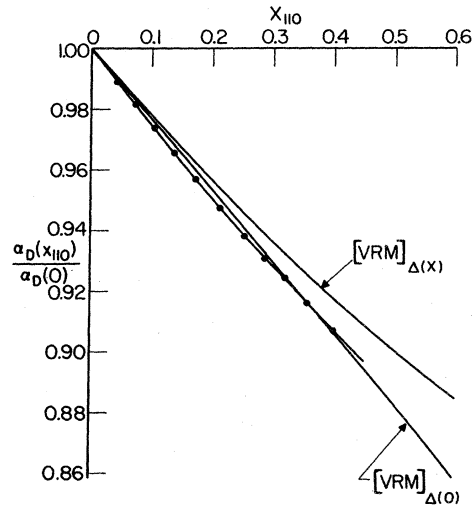

FIG. 2. $\alpha_D(x_{110})/\alpha_D(0)$ vs x_{110} for the isolated P donor in Si. The $[VRM]_{\Delta(0)}$ curve is $\Delta(x_{100})=\Delta(0)=$constant. The $[VRM]_{\Delta(x)}$ uses the $\Delta(x)$ for the [100] case given in Fig. 1. A good fit to the data is obtained for $\Delta(x)$ $=\Delta(0)(1+0.04x-0.115x^2)$.

for the $[VRM]_{\Delta(0)}$ case ($C_1=C_2=C_3=0$) shows a slope at $x_{110}=0$ which is slightly too small and which is nearly linear with a slight downward deviation from linearity which is contrary to the data deviation from linearity. The second calculated curve for the $[VRM]_{\Delta(x_{110})}$ case ($C_1=0.01$, $C_2=-0.145$, $C_3=0.042$) has a slope at x_{110} which is -0.2355—a trifle smaller than the experimental value of -0.24 ± 0.01. However, the upward deviation from linearity is too large. An excellent fit to the [110] axis data for $\alpha_D(x_{110})/\alpha_D(0)$ can be obtained with $C_1=0.04$, $C_2=-0.115$, and $C_3=0$. Although these coefficients are slightly different than for the [100] axis case the qualitative agreement is sufficiently good that one can say that the general behavior of $\Delta(x)$ is the same for both the [100] and [110] axis cases. Namely, at very small values of x, $\Delta(x)$ increases slightly, then goes through a maximum, and finally decreases in magnitude for larger x values. It should be emphasized that the two cases $[VRM]_{\Delta(0)}$ and $[VRM]_{\Delta(x)}$ differ in their prediction of the deviation of $E_{GS}(x)$ from $E_{GS}(0)$ with x. The $[VRM]_{\Delta(0)}$ case leads to an increase in the magnitude of $E_{GS}(x)$ with x (E_{GS} becomes more negative) while the $[VRM]_{\Delta(x)}$ case leads to a decrease in the magnitude of $E_{GS}(x)$ at large x values after a very small increase at the smallest x values. The behavior of $\alpha_D(x)/\alpha_D(0)$ and $E_{GS}(x)$ are mutually consistent. A decrease in $E_{GS}(x)$ should eventually lead to an increase in $\alpha_D(x)/\alpha_D(0)$ after the linear effect is overcome at larger x values. The effect is transparent for the [100] case with the minimum a dominant feature of the data.

The [110] axis data is limited to a smaller range of x_{110} and shows no minimum, although a minimum would be expected at much larger x_{110} values. For the [110] axis case the difference is more subtle and essentially corresponds to whether the deviation from linearity is upward or downward. The $[VRM]_{\Delta(0)}$ case gives a downward deviation from linearity contrary to the data while the $[VRM]_{\Delta(x)}$ case with the above C_1, C_2, and C_3 gives an upward deviation from linearity. Thus the behavior for both [100] and [110] axes shows the same qualitative change from the $[VRM]_{\Delta(0)}$ case.

Although less data was obtained for Si:Sb samples, reliable data for one dilute Sb-doped sample is shown in Fig. 3 and is compared with the theoretical results for the $[VRM]_{\Delta(0)}$ and force-fit $[VRM]_{\Delta(x)}$ cases. (Note that the VRM-EMA calculated case would be identical to that in Fig. 1.) The $[VRM]_{\Delta(0)}$ case leads to (accidentally) a slope at $x_{100}=0$ that is nearly identical to the P-donor case. The data, on the other hand show a slope $[1/\alpha_D(0)](\Delta\alpha_D/\Delta x)_{x\to0}=-0.07\pm0.01$ which is only about $\frac{1}{2}$ of the slope for the P donor. The force-fit curve $[VRM]_{\Delta(x)}$ for the Sb-donor yields $C_1=-0.0635$, $C_2=-0.050$, $C_3=0.004$. Although the qualitative behavior of $\Delta(x_{100})$ for Sb is similar to that for P in that $\Delta(x_{100})$ decreases with increasing strain for sufficiently large x_{100}, the difference in the initial slopes requires a much larger C_1 of

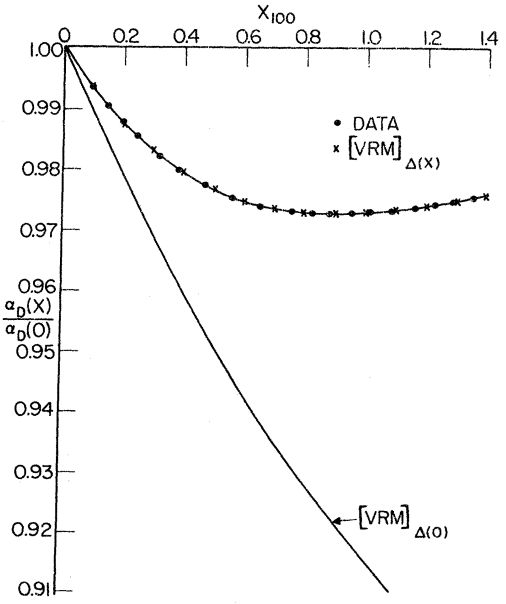

FIG. 3. $\alpha_D(x_{100})/\alpha_D(0)$ vs x_{100} for the isolated Sb donor in Si. The $[VRM]_{\Delta(0)}$ curve is for $E_{GS}(x)$ given by Eq. (16a). The $[VRM]_{\Delta(x)}$ case (force-fit to the data) is for $\Delta(x)=\Delta(0)(1-0.0635x-0.050x^2+0.004x^3)$. Note that, contrary to the P-donor case, the initial slope of the data is less than that for the calculated $[VRM]_{\Delta(0)}$ case.

opposite sign for Sb as compared to that for P. Also the C_2 for Sb is considerably smaller. These differences in the C_j for the two donors presumably represent the different core electrons for Sb and the larger size of the Sb impurity atom in Si compared to the isocoric P impurity atom. One expects the strain fields (in the absence of externally applied strain) to be of opposite sign since the P atom has a slightly smaller bonding radius than Si, and Sb has a somewhat larger bonding radius. The [110] axis results for Sb show twice the initial slope as for the [100] axis case and lead to C_j's which are qualitatively consistent with those for the [100] case in predicting that $\Delta(x_{110})$ decreases with x_{110} and $E_{GS}(x_{110})$ decreases in magnitude just as for the P donor.

We now turn to a reanalysis of the donor piezohyperfine data obtained by Wilson and Feher.[3] Since

$$a_{D\text{-hpf}}(x_{100}) \propto |\psi_{GS}(\vec{r}=0, x_{100})|^2 \propto \gamma^2(x_{100})(k_A^3\sqrt{s})$$

one obtains $a_{D\text{-hpf}}(x_{100}) \propto \gamma^2(x_{100})$ if the ground-state Bohr radius is independent of x_{100} and $\gamma^2(x_{100})$ is given by Eq. (9). From the data Wilson and Feher inferred a value of $6\Delta/\Xi_u = 1.32\times10^{-3}$ for the P donor. With $6\Delta = 12.96$ meV for P this leads to $\Xi_u = 9.8$ eV, a value approximately 15% larger than the values obtained by transport and optical studies. Employing the value $\Xi_u = 8.6$ eV obtained by Balslev[15] as a reliable value, this leads to $6\Delta/\Xi_u = 1.507\times10^{-3}$ and to an x_{100} scale 14% smaller than that used by Wilson and Feher. In Fig. 4 the original Wilson-Feher data for $a_{D\text{-hpf}}(x_{100})/a_{D\text{-hpf}}(0)$ for Si:P is shown versus x_{100}. However, after correcting for the 14% smaller x_{100} scale the data would have appeared as the dashed line based on the new x_{100} scale if one had

$$a_{D\text{-hpf}}(x_{100})/a_{D\text{-hpf}}(0) \propto \gamma^2(x_{100})$$

only with no change in $a_A(x_{100})$. However, the data can be explained by an increasing value of $a_A(x_{100})$ and the ratio of the dashed and solid curves directly determines $[a_A(x_{100})/a_A(0)]^3$. The result for $a_A(x_{100})/a_A(0)$ obtained from this analysis is shown as the dashed line in Fig. 5. One notes that only a small increase in $a_A(x_{100})$ is required to explain the drop from the dashed to the solid curve. At $x_{100}\sim 1.05$ (based on the new scale, 1.2 on the Wilson-Feher scale) the two curves differ by only 2.1%. One can show that $a_A(x)\approx a_A(0)\times(1+0.0063x_{100}^2)$ gives a relatively good fit to the data using Eqs. (8) and (9).

In Fig. 5 the relative changes in Bohr radii $a(x)/a(0)$ are shown for the A_1 state and the E_a state versus x for $x = x_{100}$. The Bohr radius $a_E(x)$ increases much more rapidly than changes in $a_A(x)$, and the increase is slightly smaller for the $[\mathrm{VRM}]_{\Delta(x)}$ case than for the $[\mathrm{VRM}]_{\Delta(0)}$ case. The more interesting and important result is for the

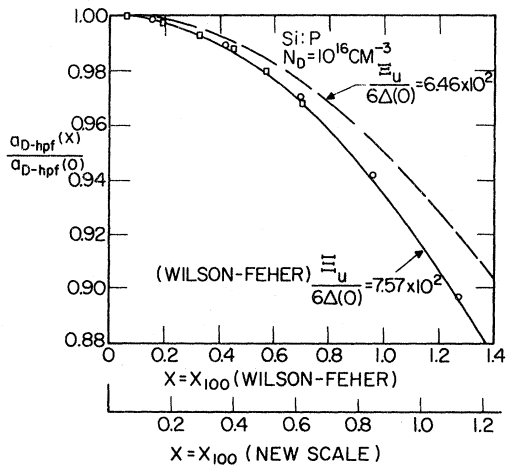

FIG. 4. $a_{D\text{-hpf}}(x_{100})/a_{D\text{-hpf}}(0)$ vs x_{100} for the isolated P donor in Si after Wilson and Feher (Ref. 3). The Wilson-Feher x_{100} scale was based on $6\Delta(0)/\Xi_u = 1.32\times10^{-3}$ while the new scale for x_{100} is based on $6\Delta(0) = 12.96$ meV (Ref. 16), $\Xi_u = 8.6$ eV (Ref. 15), and $6\Delta(0)/\Xi_u = 1.50\times10^{-3}$. The dashed curve is for constant Bohr radius case where $a_{D\text{-hpf}}(x_{100})/a_{D\text{-hpf}}(0) = \gamma^2(x_{100})$ and the new scale for x_{100}.

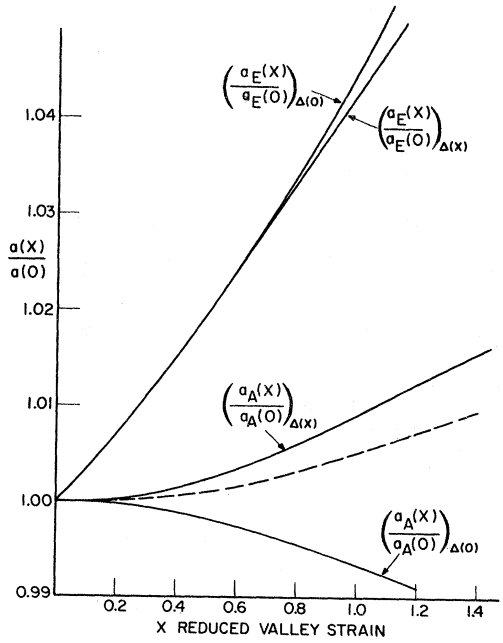

FIG. 5. The Bohr radii ratios $a_A(x)/a_A(0)$ and $a_E(x)/a_E(0)$ vs $|x_{100}|$ for the $[\mathrm{VRM}]_{\Delta(0)}$ and $[\mathrm{VRM}]_{\Delta(x)}$ cases for the isolated P donor in Si. The $[\mathrm{VRM}]_{\Delta(x)}$ curves are based on $\Delta(x) = \Delta(0)(1+0.01x-0.145x^2+0.042x^3)$. The dashed curve is the value of $a_A(x)/a_A(0)$ needed to explain the Wilson-Feher donor piezohyperfine data shown in Fig. 4 using the new x_{100} scale.

$a_A(x)$ Bohr radius. Here there is a small decrease for the $[\mathrm{VRM}]_{\Delta(0)}$ case, but significantly there is an increase for the force-fit $[\mathrm{VRM}]_{\Delta(x)}$ case. It is largely this increase in $a_A(x)/a_A(0)$, in contrast to the decrease for the $[\mathrm{VRM}]_{\Delta(0)}$ case, that accounts for the minimum and subsequent increase in $\alpha_D(x_{100})/\alpha_D(0)$ for $x_{100} > x_{100}^{\min}$ even though $a_E(x)$ is increasing more rapidly than $a_A(x)$. The increase in $a_A(x)$ is the more important effect for the range of x_{100} covered in the experiments ($x_{100} < 1.2$), since at $x_{100} \sim 1$ $\gamma^2(x_{100}) \sim 0.95$ and $\beta^2(x_{100}) = 0.05$, although the cross term proportional to $\gamma(x)\beta(x) \sim 0.25$ will play an important role also in determining $\alpha_D(x_{100})/\alpha_D(0)$. The dashed line in Fig. 5 is the value of $a_A(x)/a_A(0)$ required to fit the Wilson-Feher P-donor piezohyperfine data with the x_{100} scale based on $\Xi_u = 8.6$ eV. It is very encouraging that these two different types of experimental data both suggest that $a_A(x_{100})$ increases with x_{100}, even if the magnitude of the increase is somewhat less when inferred from the hyperfine data. One should take into account the fact that the hyperfine data depend on the $\vec{r} = 0$ value of the wave function $\psi_{GS}(\vec{r}, x_{100})$ while the polarizability shift $\alpha_D(x_{100})/\alpha_D(0)$ depends on matrix elements which emphasize the outer portion of $\psi_{GS}(\vec{r}, x_{100})$ in addition to depending on $E_{GS}(x_{100})$. Since the envelope function for the $1s$-A_1 state should contain a linear combination of exponentials with different Bohr radii from small values up to $a_A(x)$, it is not surprising that two different experiments yield different magnitudes of $a_A(x_{100})/a_A(0)$.

In Fig. 6 we show the strain dependence of the Sb-donor Bohr radii $a_E(x)$ and $a_A(x)$ for the [100] axis-strain case. Although the results are qualitatively similar to those for the P donor there are some quantitative differences. Because of the much larger C_1 for Sb the $a_E(x)$ for the $[\mathrm{VRM}]_{\Delta(0)}$ and $[\mathrm{VRM}]_{\Delta(x)}$ cases exhibit a much larger difference which starts at much smaller values of x_{100}. It is clear from Fig. 5 that for the P donor, $a_E(x)$ varies more linearly with x_{100} while $a_A(x)$ varies more nearly quadratically with x_{100}. For Sb the large C_1 term has a much larger effect on $a_E(x)$ and also causes the $[a_A(x)/a_A(0)]_{\Delta(x)}$ case to be less quadratic (i.e., it contains a linear component) than for P. The curvature of the Sb $[a_A(x)/a_A(0)]_{\Delta(x)}$ curve for larger values of x_{100} is opposite to that for the P donor.

The ground-state energy variation $E_{GS}(x_{100})$ for the P donor is shown in Fig. 7 for the $[\mathrm{VRM}]_{\Delta(0)}$ case (same as Wilson-Feher result—see their Fig. 1) and the $[\mathrm{VRM}]_{\Delta(x)}$ case. The energy $E_{GS}(x_{100})$ clearly decreases in magnitude (becomes less negative) for $x_{100} > 0.2$, although there is a very slight increase at values of x_{100} ($x_{100} < 0.07$). As already stated, the decrease in $E_{GS}(x_{100})$ is qualitatively consistent with the increase in $a_A(x_{100})$ and in $\alpha_D(x_{100})/\alpha_D(0)$ for $x_{100} > x_{100}^{\min}$. From the viewpoint of second-order perturbation theory it might seem surprising that the admixture of the $1s$-E_a

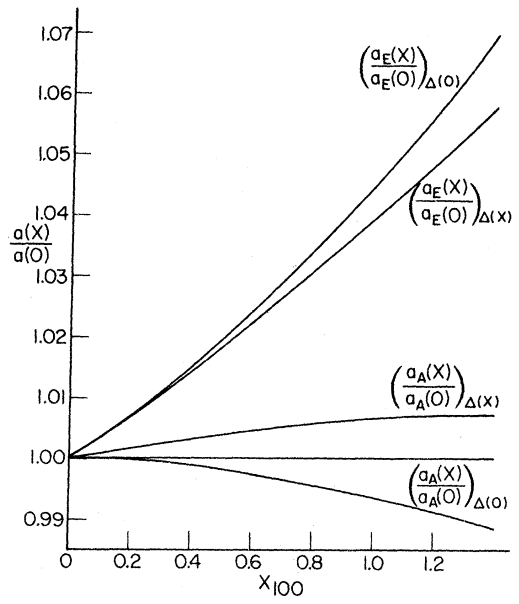

FIG. 6. The Bohr radii ratios $a_A(x)/a_A(0)$ and $a_E(x)/a_E(0)$ vs x_{100} for the $[\mathrm{VRM}]_{\Delta(0)}$ and $[\mathrm{VRM}]_{\Delta(x)}$ cases for the isolated Sb donor in Si. The $[\mathrm{VRM}]_{\Delta(x)}$ curves are based on $\Delta(x) = \Delta(0)(1 - 0.0635x - 0.050x^2 + 0.004x^3)$.

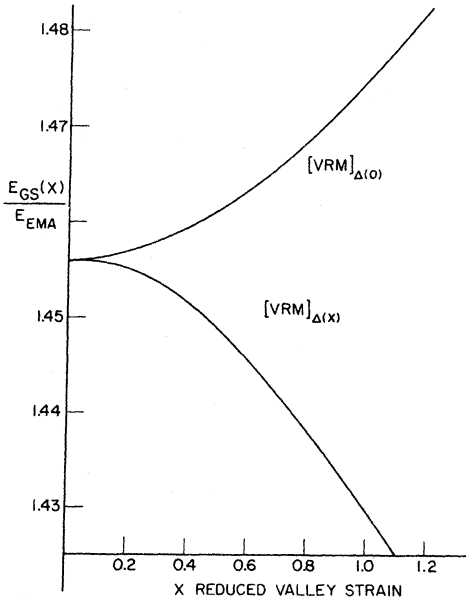

FIG. 7. The ground-state energy ratio $E_{GS}(x)/E_{EMA}$ vs x_{100} for the isolated P donor in Si for the $[\mathrm{VRM}]_{\Delta(0)}$ case and the $[\mathrm{VRM}]_{\Delta(x)}$ case. The latter case is for $\Delta(x) = \Delta(0)(1 + 0.01x - 0.145x^2 + 0.042x^3)$.

excited state by strain could raise (make less negative) the energy $E_{GS}(x_{100})$ rather than lower it as expected. The reason is that the first-order correction to $E_{GS}(x_{100})$ [η in Eq. (17a)] becomes smaller in magnitude with increasing x_{100} since we have assumed all the valley-valley coupling matrix elements have the same strain dependence as $\Delta(x)$ [i.e., $\eta(x) \propto \Delta(x)$]. The behavior of $E_{GS}(x_{100})$ for the Sb-donor case is qualitatively similar to that in Fig. 7 but with quantitative differences like those between Figs. 5 and 6.

IV. DISCUSSION AND CONCLUSIONS

The calculation of the uniaxial strain-dependent donor polarizability $\alpha_D(x)$ using Eq. (4) and the Hassé approach [yielding Eq. (11)] has only produced good agreement with the experimental data after force-fitting the valley-valley coupling matrix element $\Delta(x)$. This approach has also led to good qualitative agreement of the strain dependence of the $1s$-A_1 state Bohr radius $a_A(x)$ inferred from $\alpha_D(x_{100})$ and the donor piezohyperfine results for $|\psi_D(\vec{r}=0,x)|^2$. However, it is not easy to establish independently the reliability of the Hassé approach, which in our particular case (1) neglects the central-cell potential contribution to the matrix elements A, B, and C in Eq. (11), and (2) neglects the intervalley coupling terms in λ_1, λ_2, λ_3, A, B, and C [but not in $E_{GS}(x)$]. For the single Bohr radius envelope functions used, the neglect of the central-cell correction contribution to A is an excellent approximation. The correction is less than 0.5% for A and is much smaller for B and C. The neglect of the intervalley terms [except for $E_{GS}(x)$] is harder to estimate and depends critically on the nature of the envelope functions. Again we believe the intervalley contributions to λ_1 and A are less than 1% and are even smaller for λ_2, λ_3, B, and C. The major effect of $U_D(\vec{r})$ and the intervalley contributions is on $E_{GS}(x)$ and these effects on $E_{GS}(x)$ have been explicitly included in a phenomenological manner in Eq. (16a). A comparison, however, can be made with other calculations for the zero-strain case and for the zero-strain EMA case.

For the EMA case with no intervalley coupling, Dexter[10] has calculated $\alpha_{EMA}=\frac{1}{3}(\alpha_{\parallel}+2\alpha_{\perp})=4.328\times10^5$ Å^3. This result is just $2\frac{1}{2}$% larger than the value $\frac{9}{2}\epsilon_h a_e^3 = 4.216\times10^5$ Å^3 based on the isotropic Bohr radius $a_e = 20.18$ Å. For the EMA case Eq. (11) yields a value of α_{EMA} about 1% larger than the isotropic value and in close agreement with Dexter's result. Since Eq. (11) yields a many-valley result, with the approximations mentioned above, it might be considered a more reliable result for the donor many-valley wave function in Si. For the P donor with $U_D(\vec{r})$ included [$E_D = 1.456 E_{EMA}$, $E_{GS}(0) = E_D$], Eq. (11) yields $\alpha_D(x=0) = 1.74\times10^5$ Å^3, a value about 45% larger than the P-donor experimental value for α_D ($\alpha_D = 1.2\times10^5$ Å^3) given in I and by Capizzi *et al.*[21] Lipari and Dexter,[8] employing a single-valley approach with an envelope function consisting of a sum of exponentials with Bohr radii extending from the order of $a_A(0)$ down to the size of the central cell, have calculated a value for the P donor of $\alpha_D = 1.2\times10^5$ Å^3 which is in excellent agreement with the experimental values. Although the Lipari and Dexter $\psi(\vec{r},x=0)$ is significantly too large at $\vec{r}=0$, it nevertheless must be substantially correct at the larger values of $r \sim a_A(0)$ in order to produce the correct value of the polarizability which emphasizes the outer portion of $\psi_{GS}(\vec{r},x)$. For an envelope function of the form $F(r) = \sum C_i (\pi a_i^3)^{-1/2} \times e^{-r/a_i}$, a coefficient of $C_0 \sim 0.83$ for the exponential with Bohr radius $a_A(0)$ [$a_A(0) \propto 1/k_A(0)$ as given by Eq. (7a)] will explain the value of $\alpha_D(0)$ for P if the smaller Bohr radii components in $F(r)$ make a negligible contribution $\alpha_D(0)$. It seems clear then that $\psi_{GS}(\vec{r},x=0)$ in Eq. (4) will give too large a value of $\alpha_D(0)$ because it uses a single Bohr radius envelope function. A calculation of the donor polarizabilities for shallow donors in Si and Ge by Palaniyandi[22] using both spherical and spheroidal band approximations and one- and two-parameter trial wave functions obtains very similar results for $\alpha_D(0)$ to those obtained here. This calculation also uses only a single Bohr radius envelope function. Palaniyandi obtains, for the spheroidal band case, with a two-parameter trial function analogous to ours, $\alpha_D(0) = 1.74\times10^5$ Å^3 for Si:P and $\alpha_D(0) = 2.01\times10^5$ Å^3 for Si:Sb—both in excellent agreement with our results for $\alpha_D(0)$. This strongly suggests that it is essential to use an envelope function containing a sum of exponentials, as done by Lipari and Dexter,[8] to obtain good quantitative results for $\alpha_D(0)$.

The question of the strain dependence of $\alpha_D(x)/\alpha_D(0)$ is another question. It is our judgement that the calculated ratio $\alpha_D(x)/\alpha_D(0)$ using Eq. (4), Eq. (11), and single Bohr radius envelope function gives a considerably more accurate result than the absolute value $\alpha_D(x)$. If one were to employ an isotropic envelope function with various exponentials of weight C_i, one would also in principle have to consider the C_i as strain dependent implying that the relative shape of $F(r,x)$ could change with uniaxial strain. A simplifying assumption would be to assume only strain-dependent Bohr radius $a_i(x)$, but constant C_i. For the case that $\alpha_D(x)$ results mostly from the outermost exponential with Bohr radius $a_A(x)$, then the C_i would cancel out in both numerator and denominator of $\alpha_D(x)/$

$\alpha_D(0)$, leading to a result essentially in agreement with our calculation. For the calculation of a property such as $\alpha_D(x)/\alpha_D(0)$ which emphasizes the strain dependence of the outer or large-r portion of $\psi_{GS}(\vec{r},x)$, the present approach should be reasonable.

An earlier study of the Si^{29} piezohyperfine Fermi contact constants by Hale and Castner[23] for Si^{29} nuclei at positions $\vec{r}_l$ with respect to the donor nucleus at $\vec{r}=0$ has yielded extensive information on $|\psi_{GS}(\vec{r}_l,x)|^2$. This very detailed information on $\psi_{GS}(\vec{r}_l,x)$ at many different lattice sites gives much more information on the strain dependence of $\psi_{GS}(\vec{r},x)$ than $\alpha_D(x)/\alpha_D(0)$. The original consideration of the changes in $|\psi_{GS}(\vec{r}_l,x)|^2$ with strain was based on the approach given in I with strain-dependent Bohr radii for the stress-raised and lowered valleys. These changes in $|\psi_{GS}(\vec{r}_l,x)|^2$ with strain will be reconsidered using the $\psi_{GS}(\vec{r},x)$ in Eq. (4) in a future manuscript.

An elegant, more sophisticated many-valley theory of the shallow donor wave function $\psi_{GS}(\vec{r},x)$ has been given by Ivey and Mieher[24] and applied to the Si^{29} Fermi contact constants $a_{hpf}(\vec{r}_l,x)$ for $x=0$ and finite x. Their approach goes beyond the EMA and explicitly takes account of the variation of the Si conduction-band Bloch functions away from the conduction minima at k_0. This then, leads effectively to a complex envelope function $F_c(\vec{r},x)$ with an imaginary component that varies from site to site and is not simply proportional to the real part of $F_c(\vec{r},x)$. While this complex $F_c(\vec{r},x)$ has been shown to be very important for the $a_{hpf}(\vec{r},x)$ at certain Si^{29} sites it is uncertain how this complex $F_c(\vec{r},x)$ would affect the quantity $\alpha_D(x)/\alpha_D(0)$. The neglect of explicit stress-induced changes in the Bloch functions suggests that the strain dependence of $F_c(\vec{r},x)$ would be the same for both the real and imaginary components of $F_c(\vec{r},x)$. Further work is required to determine the effects of the $\mathrm{Im}[F_c(\vec{r},x)]$ on $\alpha_D(x)$.

In summary this work has given an alternative strain-dependent many-valley wave function which can successfully explain the donor polarizability changes with uniaxial stress if strain-dependent valley-valley coupling matrix elements are considered. This new approach gives new information on how the ground-state energy $E_{GS}(x)$ and the $1s$-A_1 state Bohr radius $a_A(x)$ vary with strain and demonstrates that the $a_A(x)$ dependence is consistent with a reinterpretation of the Wilson-Feher piezohyperfine Fermi contact constants for the P donor in Si.

ACKNOWLEDGMENTS

The authors would especially like to thank R. Bitler for programming the calculation of $\alpha_D(x)/\alpha_D(0)$ and performing many of the numerical calculations. W. Shafarman is also thanked for assistance with the numerical calculations. This work was supported in part by National Science Foundation Grant No. DMR77-20450.

APPENDIX A: MATRIX ELEMENTS FOR THE DONOR POLARIZABILITY-[100] AXIS STRESS

The wave function ψ_t in Eq. (10), where $\psi_{GS}(\vec{r},x)$ is given by Eq. (4), leads to the matrix elements λ_1, λ_2, λ_3, A, B, and C already defined in the text. λ_1 has already been discussed in Sec. II. Analogous to the expression for $\lambda_1(x)$ in Eq. (14) one finds similar expressions to Eq. (14) for $\lambda_2(x)$ and $\lambda_3(x)$ with the subscripts 1 replaced by 2 and 3, respectively. The expressions for $\lambda_i^{\parallel}(k)$ for $i=1,2,3$ are given by

$$\lambda_1^{\parallel}(k)=\frac{1}{sk^2};\lambda_1^{\parallel}(k_A,k_E)=\frac{k_A^{3/2}k_E^{3/2}}{s[(k_A+k_E)/2]^5}, \tag{A1}$$

$$\lambda_2^{\parallel}(k)=\frac{15}{2}\frac{1}{sk^4};\lambda_2^{\parallel}(k_A,k_E)=\frac{k_A^{3/2}k_A^{3/2}}{s[(k_A+k_E)/2]^7}, \tag{A2}$$

$$\lambda_3^{\parallel}(k)=\frac{5}{2}\frac{1}{sk^3};\lambda_3^{\parallel}(k_A,k_E)=\frac{k_A^{3/2}k_E^{3/2}}{s[(k_A+k_E)/2]^6}, \tag{A3}$$

where $k=k_A$ for the $\langle\cdots A_1|\cdots A_1\rangle$ matrix elements and $k=k_E$ for the $\langle\cdots E_a|\cdots E_a\rangle$ matrix elements. The $\lambda_i^{\perp}(k)$ and $\lambda_i^{\perp}(k_A,k_E)$ are just s times the respective $\parallel$ component terms. The matrix element $A=\langle z\psi_{GS}|H|z\psi_{GS}\rangle$ will be given by

$$A=\gamma^2(x)\langle zA_1|H|zA_1\rangle+\beta^2(x)\langle zE_a|H|zE_a\rangle + 2\beta(x)\gamma(x)\langle zE_a|H|zA_1\rangle.$$

Keeping only the intravalley contributions to A and separating H into kinetic energy and potential energy contributions ($H=T+V$) we obtain

$$\begin{aligned}A=&\gamma^2(x)[\tfrac{1}{3}A_T^{\parallel}(k_A)+\tfrac{2}{3}A_T^{\perp}(k_A)+\tfrac{1}{3}A_V^{\parallel}(k_A)+\tfrac{2}{3}A_V^{\perp}(k_A)]\\&+\beta^2(x)[\tfrac{1}{6}A_T^{\parallel}(k_E)+\tfrac{5}{6}A_T^{\perp}(k_E)+\tfrac{1}{6}A_V^{\parallel}(k_E)+\tfrac{5}{6}A_V^{\perp}(k_E)]\\&+\frac{\sqrt{2}\gamma(x)\beta(x)}{3}[A_T^{\parallel}(k_A,k_E)-A_T^{\perp}(k_A,k_E)\\&\qquad+A_V^{\parallel}(k_A,k_E)-A_V^{\perp}(k_A,k_E)],\end{aligned} \tag{A4}$$

where $A_T^{\parallel}=\langle zF_z|T|zF_z\rangle$, $A_T^{\perp}=\langle zF_x|T|zF_x\rangle=\langle zF_y|T|zF_y\rangle$, etc. The expressions for the matrix elements for B and C have the identical form to Eq. (A4) but with $A_T^{\parallel}$ replaced by $B_T^{\parallel}$ or $C_T^{\parallel}$, $A_V^{\parallel}$ by $B_V^{\parallel}$ or $C_V^{\parallel}$, etc. The (k_A,k_E) dependence is also explicitly shown in (A4). The $\gamma^2(x)$ term depends only on k_A, the $\beta^2(x)$ term only on k_E, and the $\gamma(x)\beta(x)$ cross terms on both k_A and k_E. The various required kinetic energy integrals are

given by

$$A_T^{\parallel}=\frac{\hbar^2}{2m_l}\frac{p(s)}{s};\ B_T^{\parallel}=\frac{\hbar^2}{2m_l}\frac{7p(s)}{2k^2s};\ C_T^{\parallel}=\frac{\hbar^2}{2m_l}\frac{3p(s)}{2ks}$$

$$A_T^{\perp}=\frac{\hbar^2}{2m_l}q(s);\ B_T^{\perp}=\frac{\hbar^2}{2m_l}\frac{7q(s)}{2k^2};\ C_T^{\perp}=\frac{\hbar^2}{2m_l}\frac{3q(s)}{2k},\tag{A5}$$

where $p(s)=[(3s/5)+(2m_l/5m_t)]$ and $q(s)=[(s/5)+(4m_l/5m_t)]$. The k dependence of the $\gamma(x)\beta(x)$ cross terms is considerably more complicated than indicated by Eq. (A5), and these are shown below.

$$A_T^{\parallel}\text{ and }A_T^{\perp}k^0\to\frac{k_A^{5/2}k_E^{5/2}}{[(k_A+k_E)/2]^5}$$

$$B_T^{\parallel}\text{ and }B_T^{\perp}k^{-2}\to\frac{k_A^{3/2}k_E^{3/2}}{7[(k_A+k_E)/2]^7}\left[15k_Ak_E-8\left(\frac{k_A+k_E}{2}\right)^2\right]\tag{A6}$$

$$C_T^{\parallel}\text{ and }C_T^{\perp}k^{-1}\to\frac{k_A^{3/2}k_E^{3/2}}{3[(k_A+k_E)/2]^6}\left[5k_Ak_E-2\left(\frac{k_A+k_E}{2}\right)^2\right].$$

The potential terms A_V, B_V, etc. are calculated neglecting the donor-dependent central-cell terms as discussed in Sec. II. The matrix elements take the form

$$A_V^{\parallel}=-\frac{3}{4}\frac{e^2f(s)}{4\varepsilon_h ks};\ B_V^{\parallel}=-\frac{15}{4}\frac{e^2f(s)}{\varepsilon_hk^3s};\ C_V^{\parallel}=-\frac{3}{2}\frac{e^2f(s)}{\varepsilon_hk^2s}\tag{A7a}$$

$$A_V^{\perp}=-\frac{3}{8}\frac{e^2g(s)}{\varepsilon_hk};\ B_V^{\perp}=-\frac{15}{8}\frac{e^2g(s)}{\varepsilon_hk^3};\ C_V^{\perp}=-\frac{3}{4}\frac{e^2g(s)}{\varepsilon_hk^2},\tag{A7b}$$

where

$$f(s)=\left(\frac{s}{s-1}\right)^{3/2}\left[\sin^{-1}\left(\frac{s-1}{s}\right)^{1/2}-\left(\frac{s-1}{s}\right)^{1/2}\frac{1}{\sqrt{s}}\right]\tag{A8a}$$

and

$$g(s)=\left(\frac{s}{s-1}\right)^{1/2}\left[\left(1-\frac{1}{(s-1)}\right)\sin^{-1}\left(\frac{s-1}{s}\right)^{1/2}+\frac{1}{\sqrt{s-1}}\right].\tag{A8b}$$

Using only the effective-mass potential $V(r)=-e^2/\varepsilon_hr$ and minimizing the energy of the single valley with respect to s one obtains

$$\left(\frac{s}{s-1}\right)^{1/2}\sin^{-1}\left(\frac{s-1}{s}\right)^{1/2}=\sqrt{s}\,\frac{(s+2m_l/m_t)}{(s^2+2m_l/m_t)}.\tag{A9}$$

With Eq. (A9), $f(s)$ and $g(s)$ take the form

$$f(s)=\frac{s^{1/2}(2m_l/m_t)}{(s^2+2m_l/m_t)};\ g(s)=\frac{2s^{1/2}(s+m_l/m_t)}{(s^2+2m_l/m_t)}.\tag{A10}$$

APPENDIX B: [110] STRESS-AXIS MATRIX ELEMENTS

The only changes that occur for this case occur because of the different $C_j(x)$ as described in Sec. II. The new matrix elements in $\lambda_1(x)$ take the form

$$\langle z\psi_{E_a}|z\psi_{E_a}\rangle=\tfrac{2}{3}\lambda_1^{\parallel}(k_E)+\tfrac{1}{3}\lambda_1^{\perp}(k_E),\tag{B1a}$$

and

$$\langle z\psi_{E_a}|z\psi_{A_1}\rangle=-\frac{\sqrt{2}}{3}[\lambda_1^{\parallel}(k_A,k_E)-\lambda_1^{\perp}(k_A,k_E)],\tag{B1b}$$

while the $\langle z\psi_{A_1}|z\psi_{A_1}\rangle$ term remains the same. The numerical coefficients in Eq. (B1a) are different than those in the $\beta^2(x)$ term of Eq. (14) [or Eq. (13b)]. The cross term proportional to $\langle z\psi_{E_a}|z\psi_{A_1}\rangle$ has changed sign and is a factor of two larger [compare Eq. (B1b) with Eq. (13c)]. The sign of $\beta(x_{110})$ has also changed sign and is opposite to that of $\beta(x_{100})$. Hence the magnitude of cross term explains the different magnitude of the initial slope (x_{100} and $x_{110}\to0^+$) of $[1/\alpha_D(0)\times\Delta\alpha_D(x)/\Delta x]$.

The other quantities of λ_2, λ_3, A, B, and C will all change in an exactly similar matter with only the numerical coefficients [identical to those in Eqs. (B1a) and (B1b) changing for the $\beta^2(x)$ term and the cross term].

APPENDIX C: THE VALLEY-ORBIT MATRIX

The generalized valley-orbit matrix for an arbitrary strain along a [100] axis will take the form

$$H_{VO}=-\begin{vmatrix} x & -x & y & -y & z & -z\\ -s'/3 & \Delta_0 & \Delta_a & \Delta_a & \Delta_a & \Delta_a\\ \Delta_0 & -s'/3 & \Delta_a & \Delta_a & \Delta_a & \Delta_a\\ \Delta_a & \Delta_a & s'/6 & \Delta_0' & \Delta_a' & \Delta_a'\\ \Delta_a & \Delta_a & \Delta_0 & s'/6 & \Delta_a' & \Delta_a'\\ \Delta_a & \Delta_a & \Delta_a' & \Delta_a' & s'/6 & \Delta_0'\\ \Delta_a & \Delta_a & \Delta_a' & \Delta_a' & \Delta_l' & s'/6 \end{vmatrix},\tag{C1}$$

where $s' = \Xi_u(s_{11} - s_{12})\sigma_s$. Δ_0 is the valley-orbit matrix element between the stress-raised (tension, $\sigma_s > 0$) x and $-x$ valleys while Δ_0' is that between the stress-lowered y and $-y$ and z and $-z$ valleys. Δ_a is the matrix element between the adjacent valleys split apart by the stress [i.e., between $(x, -x)$ and $(y, -y, z - z)$] while Δ_a' is the matrix element between the adjacent stress-lowered valleys [i.e., between $(y, -y)$ and $(z - z)$]. In principle Δ_0, Δ_0', Δ_a, and Δ_a' are all different functions of the valley strain $x_{100}(x_{100} \propto s')$. In the limit $x_{100} = 0$, $\Delta_0' = \Delta_0 = \Delta_a(1 + \delta)$ and $\Delta_a' = \Delta_a$, one has the form of H_{VO} given by Wilson and Feher.[3] If one solves for the eigenvalues W of this matrix for arbitrary s' one obtains the result

$$W = \frac{s'}{12} - \frac{1}{2}(\Delta_0' + \Delta_0 + 2\Delta_a') \pm \frac{1}{2}\left[\left(\Delta_0' + 2\Delta_a' - \Delta_0 + \frac{s'}{2}\right)^2 + 32\Delta_a^2\right]^{1/2}, \quad \text{(C2)}$$

with the plus sign for the "E_a" state and the minus sign for E_{GS}. The energy splitting between "E_a" and E_{GS} is just given by the square root which reduces to $6\Delta(0)$ for $\Delta_a' = \Delta_a = \Delta(0)$ for $s' = 0$. One also observes that the dominant contribution to W comes from Δ_a with the next most important contribution arising from Δ_a'. Thus, it is clear that the $\Delta(x_{100})$ used in force-fitting the polarizability data $\alpha_D(x_{100})/\alpha_D(0)$ depends most importantly on $\Delta_a(x_{100})$, the adjacent-valley coupling between the stress-raised and the stress-lowered valleys.

---

*Present address: 1, Lorong Tiong Nam 6, Kuala Lumpur 02-08, Malaysia.

[1]H. S. Tan and T. G. Castner, Phys. Rev. B 23, 3983 (1981)
[2]P. J. Price, Phys. Rev. 104, 1223 (1956).
[3]D. K. Wilson and G. Feher, Phys. Rev. 124, 1068 (1961).
[4]H. Fritzsche, Phys. Rev. 125, 1560 (1962).
[5]See, for example, R. L. Aggarwal, P. Fisher, V. Mourzine, and A. K. Ramdas, Phys. Rev. 138, A882 (1965); G. D. Watkins and Frank S. Ham, Phys. Rev. B 1, 4071 (1970).
[6]J. C. Hensel, H. Hasegawa, and M. Nakayama, Phys. Rev. 138, A225 (1965).
[7]M. Cardona, W. Paul, and H. Brooks, *Proceedings of the International Conference on Solid State Physics in Electronics and Telecommunications, Brussels, 1958;* J. Phys. Chem. Solids 8, 204 (1959).
[8]See, for example, N. O. Lipari and D. L. Dexter, Phys. Rev. B 18, 1346 (1978).
[9]See the references given in I (Ref. 1).
[10]D. L. Dexter, in *Proceedings of the 13th International Semiconductor Conference, Rome, 1976,* edited by F. G. Fumi (North-Holland, Amsterdam, 1977), p. 1137.
[11]C. Herring and E. Vogt, Phys. Rev. 101, 944 (1956).
[12]See the review by W. Kohn, in *Solid State Physics,* Vol. 5, edited by F. Seitz and D. Turnbull (Academic, New York, 1957).
[13]F. J. Morin, T. H. Geballe, and C. Herring, Phys. Rev. 101, 525 (1957).
[14]J. E. Aubrey, W. Gubler, J. Henningsen, and S. H. Koenig, Phys. Rev. 130, 1667 (1963).
[15]I. Balslev, Phys. Rev. 143, 636 (1966).
[16]R. L. Aggarwal and A. K. Ramdas, Phys. Rev. 137, A602 (1965).
[17]H. R. Hassé, Proc. Cambridge, Philos. Soc. 26, 542 (1930).
[18]D. L. Dexter, Phys. Rev. A 18, 862 (1978).
[9]T. G. Castner, Phys. Rev. B 21, 3523 (1980).
[20]E. B. Hale, J. Phys. Chem. Solids 34, 621 (1973).
[21]M. Capizzi, G. A. Thomas, F. DeRosa, R. N. Bhatt, and T. M. Rice, Phys. Rev. Lett. 44, 1019 (1980).
[22]E. Palaniyandi, Phys. Status Solidi 100, 321 (1980).
[23]E. B. Hale and T. G. Castner, Phys. Rev. B 1, 4763 (1970).
[24]J. L. Ivey and R. L. Mieher, Phys. Rev. B 11, 822 (1975).